DNA Detection: Finding the Limits

by

Emma Kitchner

Bachelor of Science, 2019
St. Lawrence University
New York

Submitted to the Graduate Faculty of the
College of Science and Engineering
Texas Christian University
in partial fulfillment of the requirements
for the degree of
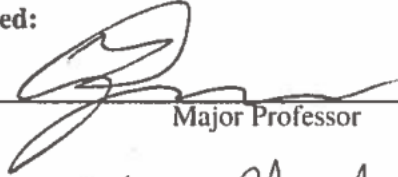
Master of Science

TCU

Fall 2021

APPROVAL

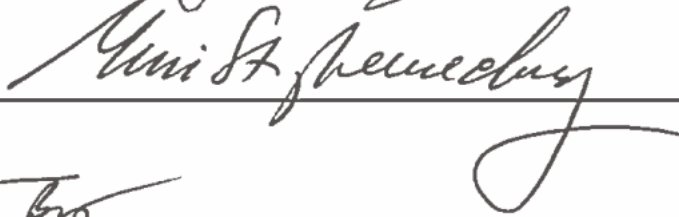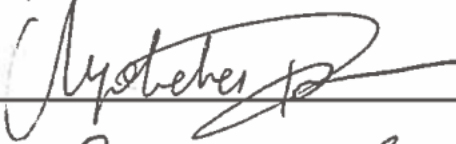## DETECTING DNA: FINDING THE LIMITS

by

Emma Kitchner

Dissertation **approved:**

_____
Major Professor

_____

_____

_____

_____

_____
For the College

Acknowledgments

I would like to thank my advisor, Dr. Zygmunt (Karol) Gryczynski, Dr. Ignacy Gryczynski, and Dr. Magdalena Bus for sharing their collective knowledge and providing guidance and support.

I am also grateful for all the help and discussions with those in my lab: Jose Chavez, Luca Ceresa, Michael Seung, Dr. Joe Kimball, and the physics graduate students.

I would lastly like to thank my family and friends for their support, especially my parents.

Table of contents

List of Figures

List of Abbreviations

1. Introduction:

DNA: Deoxyribonucleic Acid

RNA: Ribonucleic Acid

dsDNA: double-stranded Deoxyribonucleic Acid

EtBr: Ethidium Bromide

PCR: Polymerase Chain Reaction

2. Theory:

QY: Quantum Yield

ns: nanosecond

μM: micro- Molar

s: second

nm: nanometer

a.u.: arbitrary units

MHz: MegaHertz

μg/ml : microgram per milliliter

3. Materials:

°C: degrees Celcius

DI: Deionized

ml: milliliter

µm: micrometer

A.U.: Absorption Units

cm: centameter

Inc.: Incorportated

GmbH: Gesellschaft mit beschränkter Haftung (company with limited liability)

PMT: Photomultiplier Tube

TCSPC: Time Correlated Single Photon Counting

HPPD: Hybrid Picosecond Photon Detector

TRES: Time-Resolved Emission Spectra

IRF: Instrument Response Function

ms: milliseconds

PDL: Pulsed Diode Laser

PI: Princeton Instruments

4. Results:

ng/ml: nanogram per milliliter

5x: five times

PBS: Phosphate Buffered Saline

1. Introduction

Fluorescence spectroscopy and time-resolved fluorescence are primary research tools used in various fields, from environmental sensing to biomedical diagnostics [1-3]. Over the past 30 years, fluorescence has come to be one of the most sensitive detection techniques.

Fluorescence-based methods are among the preferred approaches for DNA detection because they offer high sensitivity, speed, and specificity [4]. Fluorescence detection of double-stranded DNA (dsDNA) utilizes the significant emission signal enhancement from dye-intercalators upon binding to DNA. Optical detection methods offer extensive detection flexibility and can readily be used for liquid samples (solutions).

Many intercalators (dyes) have been developed and widely utilized for DNA detection [5-11]. Practically all intercalators have a high affinity to DNA/RNA (either for a specific sequence base or general domain). These intercalators present high fluorescence signal enhancement upon interaction with DNA molecules, either single-stranded (ss) or double-stranded (ds). The emission signal of a bound probe can be easily enhanced by more than an order of magnitude. Binding typically produces a slight change in absorption and only a minor change/shift in the dye's emission spectrum. The limited access of water within the dsDNA environment stabilizes the chromophore and thus increases the quantum yield and the lifetime of the dye. A significant increase in fluorescence lifetime can be utilized to improve detection sensitivity [12,13] further. When using highly advanced time-resolved detection, Kimball et al. [12] showed an increase (close to two orders of magnitude) in sensitivity for DNA detection when using Ethidium Bromide (EtBr) as a probe.

1

Medical and biological research progress is highly dependent on developing new, improved, but more straightforward methods for sensitive detection of biomolecules. Although many advantageous detection methods have been developed, they still present insufficient sensitivity, and their practical application is even more limited when low-target detection is necessary [14]. Complex carriers and endogenous sample components can further limit the sensitive and precise detection of a target molecule. Over many years, DNA detection in various applications (e.g., biological research, diagnostics, forensics, etc.) required DNA extraction, amplification of selected DNA fragments by Polymerase Chain Reaction (PCR), separation in gel or other media, or specific signal measurement.

The collection and recovery of DNA can be very challenging, especially if a minute amount of DNA is available for such processes. One of the most common sample types left at a crime scene is touch DNA [15,16]. When a person makes direct contact with an object/item/surface, they unintentionally deposit touch DNA. The source of touch DNA is epithelial cells and free DNA. Touch DNA can be highly informative and frequently constitutes crucial evidence in criminal investigations. However, touch DNA is not visible after deposition and can be present in only trace amounts. Currently, no efficient procedure allows for the localization of touch DNA on a surface or object. Touch DNA is found in low copy numbers (<100 – 200 pg), which poses challenges to downstream DNA analysis [17-19]. Therefore, localizing and maximizing the amount of recovered DNA for subsequent analysis becomes a significant challenge. For example, forensic analyses of human DNA consider a sufficient amount of DNA template for PCR amplification to be ~ 500 pg – 1 ng (~ 76 to 152 diploid cells equivalents) [15,16].

The development of advanced detection, quantification, and imaging techniques of biomolecules [1,2,14,20-22] has made significant progress over the years. However, there is still a need to improve detection speed and precision and better quantification and imaging methods.

We present three approaches that demonstrate the potential of significant sensitivity enhancement for detecting small amounts of DNA. One method is based on the spectral change induced by an intercalator binding to DNA [4]. The second one utilizes the change in fluorescence lifetime of an intercalator upon binding to DNA [12]. Lastly, the third approach utilizes both a change in the fluorescence lifetime and a change in the emission spectrum through advanced multipulse technology.

In the first approach, spectral decomposition was applied to the overall emission signals to extract the fraction of EtBr bound to DNA. We were able to detect less than 100 pg of DNA in the cuvette. Using the second approach (time-resolved spectra) [12], we can lower the emission spectra detection limit by another order of magnitude. The third approach is more technologically advanced but is easily achievable in a typical laboratory setup. These strategies open a new direction for quick visualization of minute amounts of DNA in a sample. The capability to visualize sub-nanograms amounts of DNA in microliters of solution is demonstrated.

EtBr is one of the oldest and most common DNA markers with a specified sensitivity limit in the nanograms range. For the selected excitation wavelengths, the detection limits were tested for DNA in controlled cuvette experiments. In these controlled cuvette experiments, we applied spectral decomposition to the data to extract the fraction of EtBr bound to DNA. This process was performed for the various detection experiments, and the obtained results were compared between the various methods.

EtBr is used as it is a well-characterized model system for these experiments, and low-detection limits were achieved (sub-nanograms) [4,13]. However, by employing dyes of much higher binding affinity than EtBr, such as Ethidium Dimer, Diamond^{TM}, or YOYO, even more, negligible traces of DNA (sub-picograms) may be detectable without the need for prior DNA amplification. Such an approach will limit the unnecessary processing of samples that do not contain sufficient DNA for downstream analyses. Furthermore, it will increase the efficiency of collecting DNA from areas of interest, e.g., touched objects/surfaces, explosive devices.

2. Theory

2.1 Absorption

Valence electrons are loosely bound to the nucleus and form "molecular orbitals." These molecular orbitals are responsible for the electronic interactions between light and the molecule. Furthermore, these molecular orbital energies are quantized, similar to atomic energy levels.

When light and a molecule interact, the energy of the photon can be absorbed by the molecule. This absorption of energy can be transferred to the molecule's molecular orbital, leading to a transition to an "excited state," but only if the photon's energy and the energy required for the molecules' transition to the excited state are in resonance. This transition from the ground state to the excited state requires a discrete amount of energy, and the photon has an inherent and discrete amount of energy. This concept of discrete energy is essential because a molecule can only be in the ground state or at an excited state, meaning the molecule will absorb the photon or it will not.

The process of absorption is qualitatively explained in what is commonly known as a Jablonski diagram (Figure 2.1) [1-3].
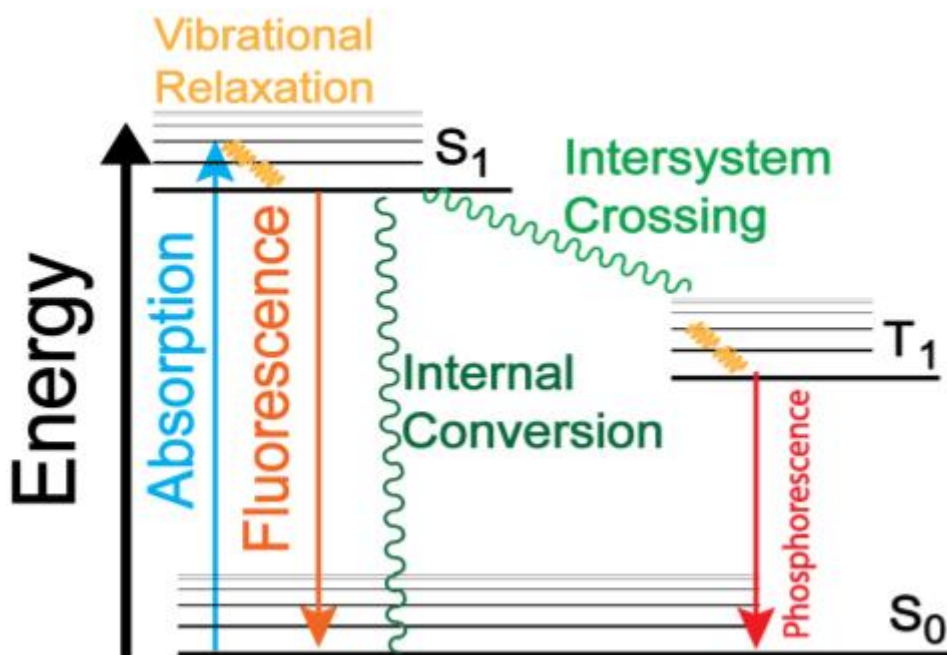
Figure 2. 1: Jablonski Diagram, sometimes referred to as Jablonski-Perrin Diagram [23].

This diagram shows a classic energetic representation of molecular energy levels. Each horizontal line represents an energy state E_i. The bold solid lines represent the ground vibrational levels of the electronic states, and the thin solid lines represent higher level vibrational and rotational energy levels. The straight arrows represent pathways involving photons, and the squiggly arrows represent non-radiative pathways.

When a molecule is in its lowest energetic state, named the ground state S_0, the molecule is characterized by a corresponding energy E_0. Light can interact with the molecules, and when the light and molecules interact, the molecule can transition to the excited state. The transition into the excited state from the ground state is called the absorption process. In particular, the absorbed energy of light ($E = h\nu$) promotes the molecule from the ground state energy E_0^k to a new energy state with quantized total energy indicated as E_i^j. The process of absorption is swift (i.e., 10^{-15} s). The difference in energy between the ground state and one of the excited states is

$$\Delta E = E_i^j - E_0^k \quad (2.1)$$

Light absorption by molecules is determined primarily by three factors [1-3]. First, the energy of the incident photon has to correspond to the energy difference of the two states (i.e., $h\nu = E_i - E_0$). Second, the intensity of the excitation light directly correlates to the number of excited molecules. Lastly, the relative orientation between the polarization of the excitation light and the molecular transition moment needs to be considered.

Absorption measurements are based upon the comparison between the intensity of the incident and the transmitted light. The intensity of light is attenuated as it crosses the sample. Figure 2.2 represents the experimental concept of absorption measurements. The intensity of light transmitted through the cuvette (leaving on the other side) and reaching the detector is indicated as I.
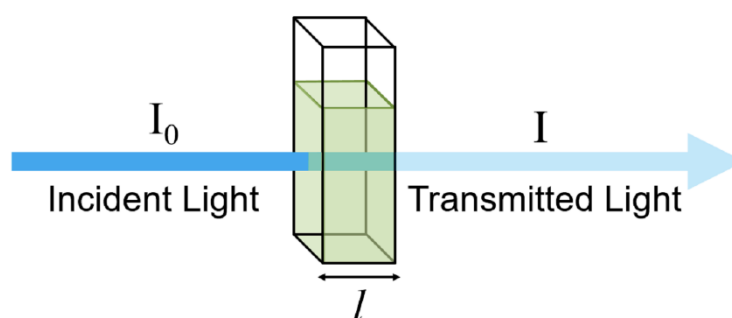
Figure 2. 2: Experimental concept of absorption measurements [24].

The intensity of the transmitted light through the sample is given via the Lambert-Beer Law:

$$I = I_0 \cdot e^{-\sigma n l} \quad (2.2)$$

Where n is the number of chromophores per unit volume, l is the path length of the sample that the light travels through (i.e., cuvette width), and σ is the absorption cross-section. The absorption cross-section is the probability the chromophore will absorb a photon. In photochemistry and photobiology, extinction coefficient is typically used instead of absorption-cross section. Extinction coefficient, ϵ, measures how well a chromophore at a concentration of one mole in a one cm layer can absorb photons at a particular wavelength [1]. Converting absorption cross-section to extinction coefficient we get,

$$\epsilon = \frac{\sigma N_A}{2.303} \quad (2.3)$$

Where N_A is Avogadro's Number ($N_A = 6.0225 x 10^{23} mol^{-1}$). Plugging Equation 2.3 back into Equation 2.2, we get a new form of Lambert-Beer Law.

$$I_T = I_0 \cdot 10^{-\epsilon Cl} \quad (2.4)$$

Where C is the concentration of the chromophore and can be calculated from the following conversion.

$$C = n * \left(\frac{1000}{N_A}\right) \quad (2.5)$$

Absorbance (A) is then defined as the argument found in the exponents in the Lamber-Beer Law (Equation 2.4).

$$A = \varepsilon\, C\, l \quad (2.6)$$

2.2 Emission

After a molecule absorbs a photon and is in the excited state, the molecule will then quickly relax to the lowest excited energy state. There are two different forms of molecule deexcitation, radiative emission (photon involved) and non-radiative deactivation (non-photon involved); see Figure 2.1. We can quantitatively describe the rate at which they occur, radiative (Γ) and non-radiative (k_{nr}).

The quantum yield of a molecule (QY) describes how well the molecule is at emitting a photon after it has absorbed a photon is,

$$QY = \frac{\# \, photons \, emitted}{\# \, photons \, absorbed} = \frac{\Gamma}{\Gamma + k_{nr}} = \frac{\Gamma}{k} \quad (2.7)$$

Where k is the sum of the radiative and non-radiative rates.

The possible radiative routes are fluorescence and phosphorescence (solid arrows in Figure. 2.1). In these cases, a photon is released, carrying the energy required for the molecule to transit to the ground state. Fluorescence is a process that occurs when there is no change in

spin multiplicity (S_1 to S_0). The time scale for fluorescence is short, on the order of 10^{-9} seconds (nanoseconds). Phosphorescence occurs when there is a change in the spin multiplicity (T_1 to S_0). This is a spin-forbidden process and therefore happens at a relatively slow rate, on the order of 10^{-4} to 10^2 seconds. Non-radiative routes in which energy can be dissipated are collisions (10^{-10} s) with surrounding molecules (heat), internal conversion (10^{-12} s), intersystem crossing (10^{-5} s) and dissociation/breaking of bonds from the molecule itself [1-3, 25].

After absorption, the molecule quickly relaxes (10^{-13} s) into the lowest excited energy state. Fluorescence occurs if a molecule then transits back to the ground state and emits a photon. The emitted photon can have less energy than the photon that the molecule absorbed due to the non-radiative energy losses, ($E = h\nu$). This change in energy between the absorbed photon and the emitted photon is manifested as Stoke's shift. The emitted photon can have a longer wavelength than the initial absorbed one (i.e., a fluorescein molecule in Figure 2.3) [1-3, 23, 25].
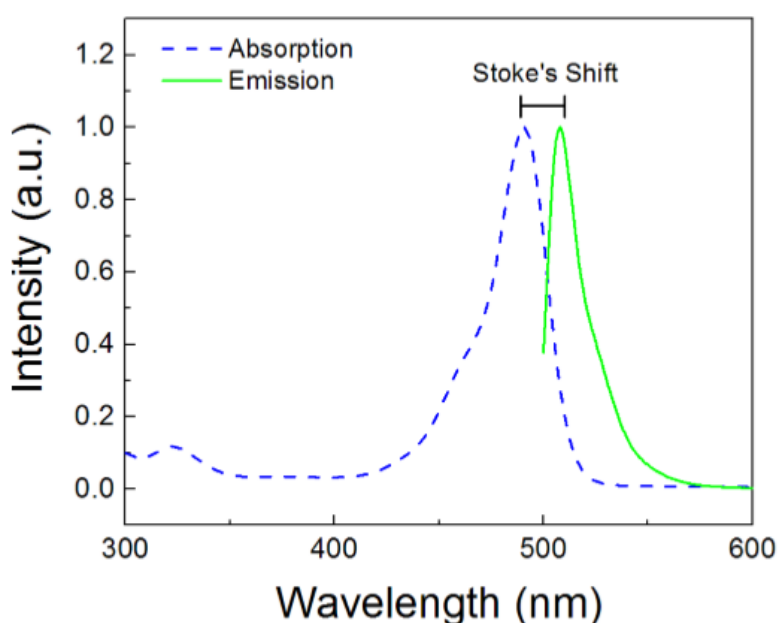
Figure 2. 3:Absorption (dotted blue) and emission (solid green) spectra of 6 µM fluorescein [23].

2.3 Lifetimes

Fluorescence lifetime is the average time the molecule spends in the excited state before it transits back to the ground state. The definition arises from the fact that the transition of an excited molecule to the ground state is a purely statistical process that can be characterized by a rate constant (probability to transition). The lifetime can then be calculated as the reciprocal of the total decay rates. [1-3, 25].

$$\tau = \frac{1}{\Gamma + k_{nr}} \quad (2.8)$$

If the initial number of molecules in the excited state is denoted as N_0, the number of molecules in the excited state as a function of time can be modeled by a first-order rate equation

$$\frac{dN(t)}{dt} = -kN_0(t) \quad (2.9)$$

Where k is the total decay rates, $k = \tau + k_{nr}$. Integrating with respect to time,

$$N(t) = N_0 e^{-kt} \quad (2.10)$$

Because the definition of a lifetime (Equation 2.8) is equivalent to $\tau = 1/k$ we get

$$N(t) = N_0 e^{-\frac{t}{\tau}} \quad (2.11)$$

Therefore, the average fluorescence lifetime of a single exponential decay is $1/slope$ when the logarithm of the intensity is plotted versus time. Figure 2.4 is an experimental demonstration of a single decay using 6 μM fluorescein [1-3, 23, 25].
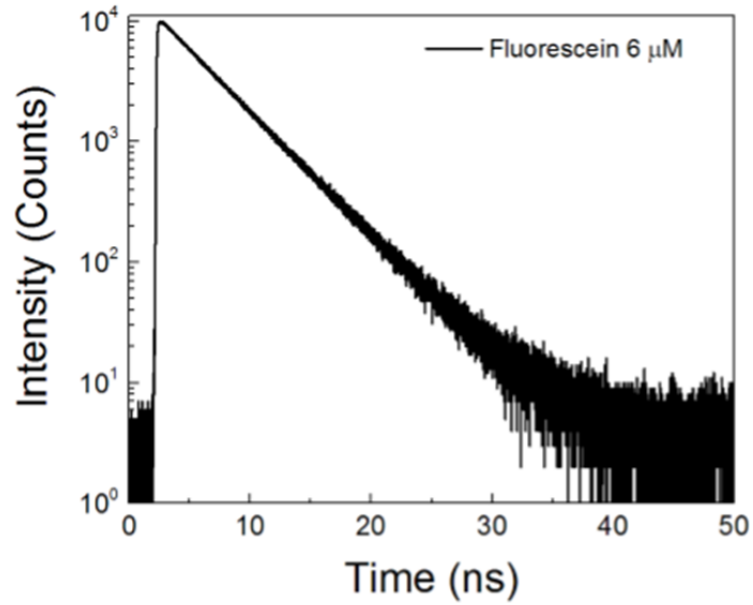
Figure 2.4. Fluorescence intensity decay of 6 μM fluorescein [23].

The intensity decay can then be found as

$$I(t) = \sum_i I_o \alpha_i e^{-t/\tau_i} \sim \sum_i N_o \alpha_i e^{-t/\tau_i} \quad (2.12)$$

2.4 Multipulse

For a system that contains two species, one short-lived and one long-lived, the measured steady state emission spectrum is a simple sum of photons emitted by the short-lived fluorophore and the long-lived fluorophore. Measured intensities represent the relative fractions of short- and long-lived fluorophores (see Figure 2.5). When using pulsed excitation, the measured steady-state spectrum reflects the same fractions of both components. However, as the excited molecules decay after the excitation pulse, the distribution of photons emitted at a different time by short-lived and long-lived fluorophores will be different. In the beginning, the dominant number of photons will be emitted by the short-lived component (the component that decays faster). As the detection time is shifted, the relative contribution of photons from the species with a longer lifetime will be increased.
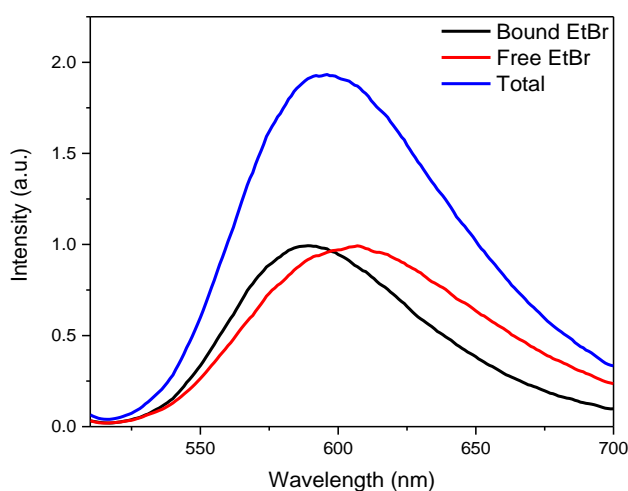
Figure 2.5. Uncorrected normalized emission spectra of free EtBr (Red) and EtBr fully bound to DNA (Black) as measured with the Delta Flex system from Horiba. The blue line represents a total (cumulative) emission of a mixture.

Consider a system composed of two emission species with different emission spectra and significantly different fluorescence lifetimes. The first one is short-lived, and the second one is long-lived. The spectra of the two species easily distinguishable, Figure 2.6.
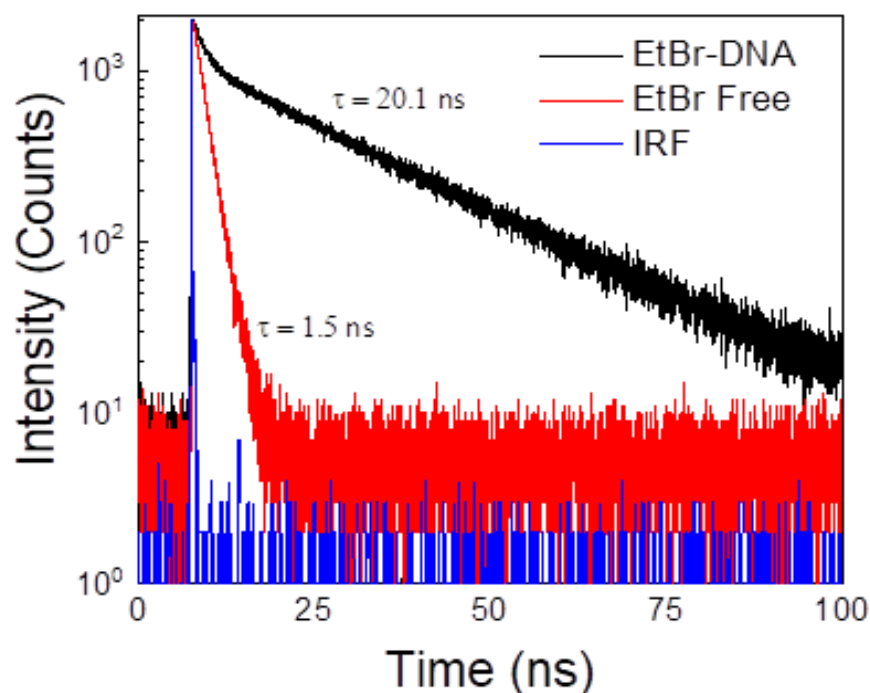
Figure 2.6. Fluorescence intensity decays for EtBr (red) and EtBr bound to DNA (blue).

Consider a mixture where a 50:50 intensity mixture can quickly still be resolved by spectral decomposition. Specifically, when using EtBr and DNA, at 485 nm excitation, EtBr increases intensity about six-fold upon binding to DNA. Therefore, the 50:50 intensity fractions represent ~8.3% of bound EtBr and almost 92% free EtBr. The goal is to detect and visualize the lowest possible fraction of EtBr bound to DNA that can be explicitly distinguished on a free (unbound) EtBr background. A dual-pronged approach was utilized in these experiments: pulse pumping with a time-gated detection mode that exclusively enhances the observed emission of the bound EtBr fraction [26-28].

Assume that the shorter wavelength emission (EtBr bound to DNA) has a fluorescence lifetime of 20 ns, and the longer wavelength emission (free EtBr) has a lifetime of 1.5 ns. A

mixture of 8:92 of bound and free EtBr will present comparable steady-state emission signals from both forms, a 50:50 ratio relative to the signal intensities, as shown in Figure 2.5.

If a burst of temporally closely spaced pulses is used as the excitation source, the population of the excited state will change after each pulse, depending on the relation between the fluorescence lifetime and the pulse separation in the burst [26-28]. For a fluorescence lifetime much shorter than the pulse separation, the fluorescence intensity will completely decay before the arrival of the next pulse, Figure 2.7.
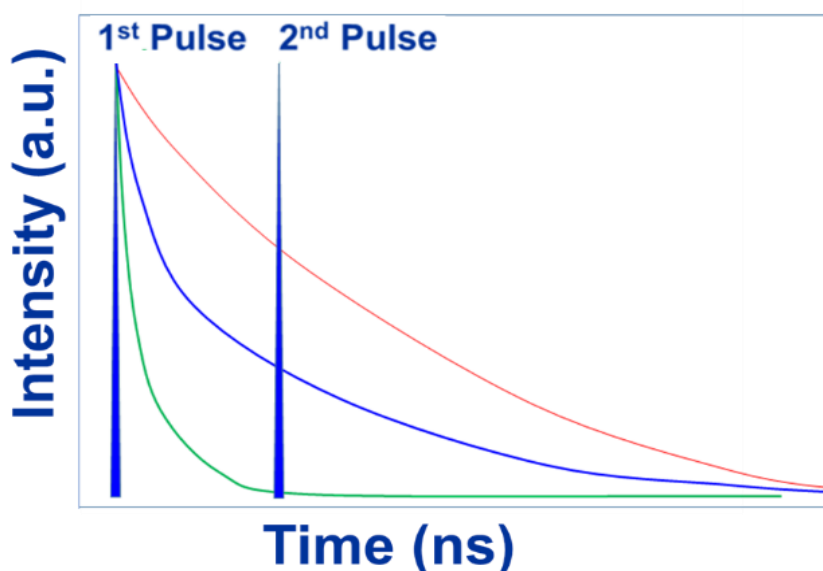
Figure 2.7. Pumping of mixed solution (blue line). The short component is not affected by the second pulse (green line). However, the long component is pumped by the second pulse (orange line) [29].

For a lifetime much longer than the time separation between excitation pulses, the molecules in the excited state will not completely decay during the time between pulses. Each sequential pulse will add to the excited state population, Figure 2.8.
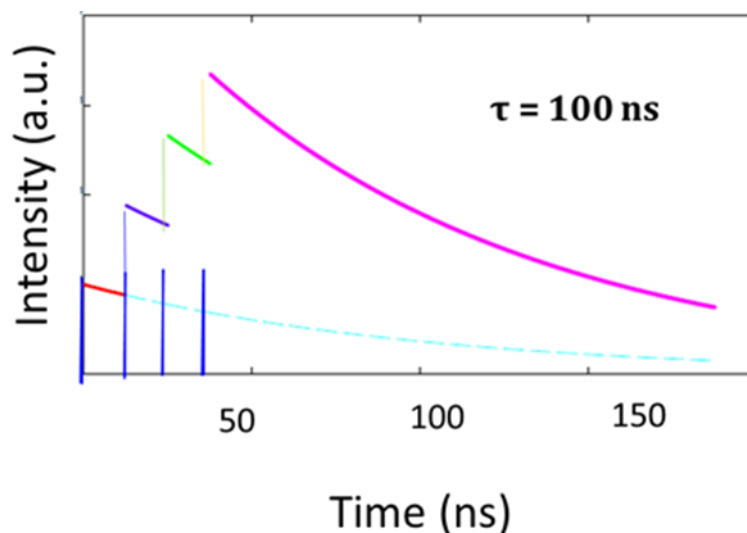
Figure 2.8. Pumping of the long component in a sample increases the lifetime intensity of the sample [29].

Effectively, measurements starting after the last pulse in the burst will detect many more excited molecules with a longer fluorescence lifetime. As presented in [26,27], the population of the excited state (emission signal) can be calculated for a short-lived (free) component and a long-lived (bound) fraction as a function of n pulses in the burst:

$$I(n) = I_o \frac{1 - e^{\frac{n\Delta t}{\tau}}}{1 - e^{\frac{\Delta t}{\tau}}} \quad (2.13)$$

Where n is the number of pulses in the burst, Δt is the separation between pulses in the burst, and τ is the fluorescence lifetime of the sample.

Figure 2.9 presents the expected change in the measured intensity after the last pulse as the number of pulses in the burst is increased. The pulse separation in the burst was designed as Δt=4 ns and considered a fluorescence lifetime of 1.5 ns for the free EtBr fraction and 20 ns for the bound to DNA EtBr fraction. The short-lived population increases by less than 10%. It stays practically constant after the second pulse, while the population of the long-lived fraction quickly increases and already triples after four pulses.

Figure 2.9. Calculated emission intensities for an increasing number of pulses in the burst for short 1.5 ns lifetime (green line) and long 20 ns lifetime (blue line).

Figure 2.10 presents simulated spectra expected from a system with 8% bound and 92% free EtBr fractions corresponding to 50:50 intensity between free (dashed black line) and bound (dashed red line). As anticipated, with 4-pulse excitation, the long-lived fraction (solid red line) significantly increases and now contributes almost three times more to the total intensity (solid green line).
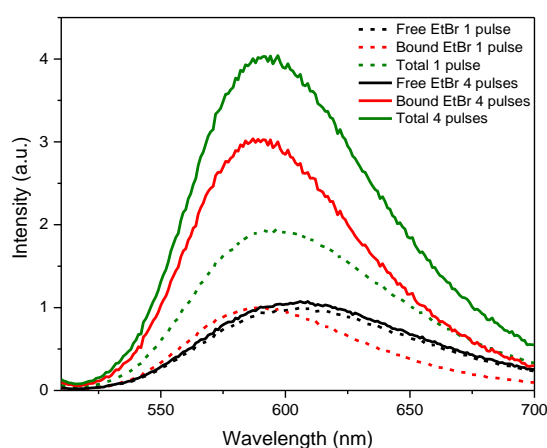
Figure 2.10. Simulated spectra as expected from the first system (8% bound and 92% free EtBr fractions corresponding to 50:50 intensity between free and bound at 485 nm excitation) single pulse excitation (dashed lines) and 4-pulse excitation (solid lines).

Next, time-gating was applied to the detection mode. In contrast to pulsing, time gating is passive, and the initial signals will only decrease. So, the sample must present a measurable

signal for the lowest intensity fraction (the long-lived component in this case) at zero time (when starting the gate). The signal of the free fraction and bound fraction will decrease accordingly to delay time for the gate opening:

$$I(t) = I_0 \int_{\Delta t}^{\infty} e^{\frac{-\tau}{t}} \ dt \quad (2.14)$$

Therefore, for a short-lived fraction, the measured intensity will decrease much faster.

Again, consider a system composed of two emission species with different emission spectra and significantly different lifetimes. The first one is the short lifetime, and the second one is the long lifetime. The spectra of the two species are similar but easily distinguishable, see Figure 2.11.
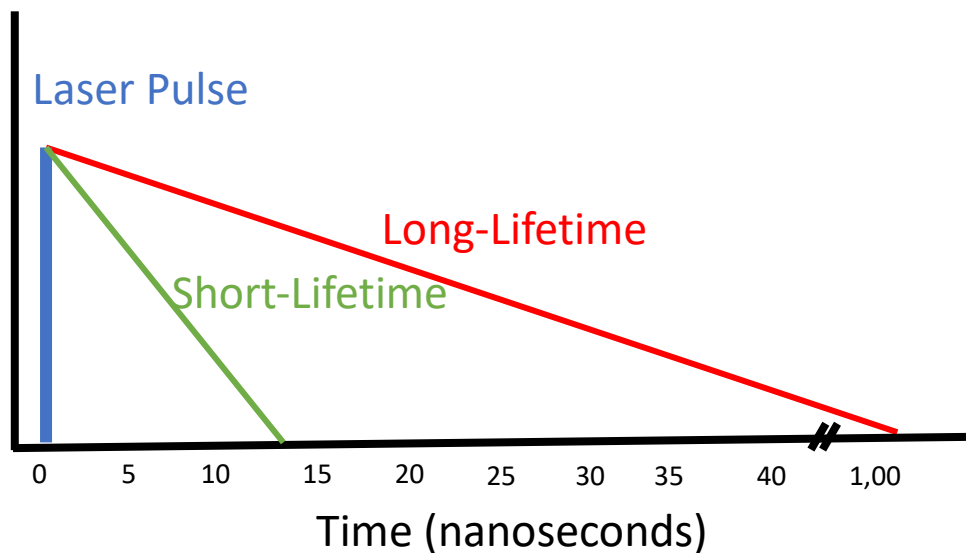
Figure 2.11. Laser pulse with two different lifetimes, short and long.

With the separable lifetimes, we can look to apply time gating to the system. Time gating works by delaying the time at which the shutter for the detector opens to receive the signal.

Time gating relies not only on the delay of the detector shutter opening but also on how long the shutter is opened. Let's consider a pulsed laser diode with a repetition rate of 10 MHz. If the detectors shutter has a delay that is set to open 5 ns after the initial pulse but remains open for 100 ns, the shutter will remain open during the second pulse. The signal collected

will still contain the pulse of the laser plus the 5 ns afterward that the shutter delay was designed the gate out.

Effectively, time gating requires controlling when the detector opens (gate time) and how long the detector remains open for (gate width).

Figure 2.12 demonstrates multiple gate delays, all with a 5 ns gate width. Figure 2.12A has a gate delay of 2 ns. The short-lifetime component dominates the signal, with only a small portion of the signal relegated to the long-lifetime component. For Figure 2.12B, in which the gate delay is 10 ns, most of the signal seems to come from the long-lived component, with only a tiny portion of the signal coming from the short-lived component. For 2.12C and 2.12D (20 ns and 40 ns gate delay, respectively), only a minuscule amount of signal will come from the short-lived component leaving the signal dominated by the long-lived component. The overall signal of the long-lived components also decreases in cases C and D as the gate delay moves further from the initial pulse. That is why it is pertinent that pulse and time gating be used in tandem when dealing with low signals (like DNA detection).
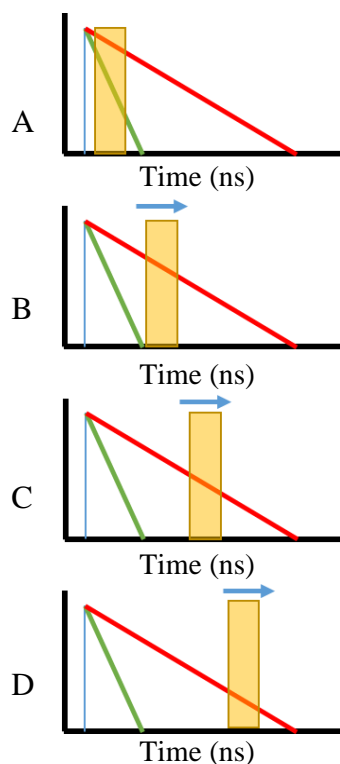
Figure 2.12. Various time gating scenarios demonstrated.

Figure 2.13 (Panels A and B) presents the expected intensities from the free and bound EtBr fractions as a function of gate time opening. The leftmost column shows simulated spectra as measured after a single pulse and no delay. Next, the expected relative intensities after four pulses are shown. The fraction of the long-lived component is tripled. The four other columns of emission spectra are (left to right) after two, five, and ten nanoseconds delay times for the gate opening with the 4-pulse excitation. For panel A (2 µg/ml), the total signal is essentially dominated by the bound fraction already after 5ns. After 10ns, the intensity is practically zero for the short-lived fraction, while the long-lived drops only about 40%. A comparable response is observed for Panel B (0.3 μg/ml), where the bound fraction was assumed to be below 0.2% and was almost indistinguishable with a single pulse. After four pulses, the trace of the long-lived fraction is a little more visible. The relative fraction of the long component increases with the delay time for gate opening, and after 10ns, the signal from the bound form dominates the observed emission.

Figure 2.13. Expected emission intensities from the free and bound EtBr fractions as a function of gate time opening for two different concentrations of DNA: 2 ug/ml (panel A) and 0.3 ug/ml (Panel B) after 4-pulse excitation burst. For comparison the left-most graphs show intensities observed with single pulse excitation.

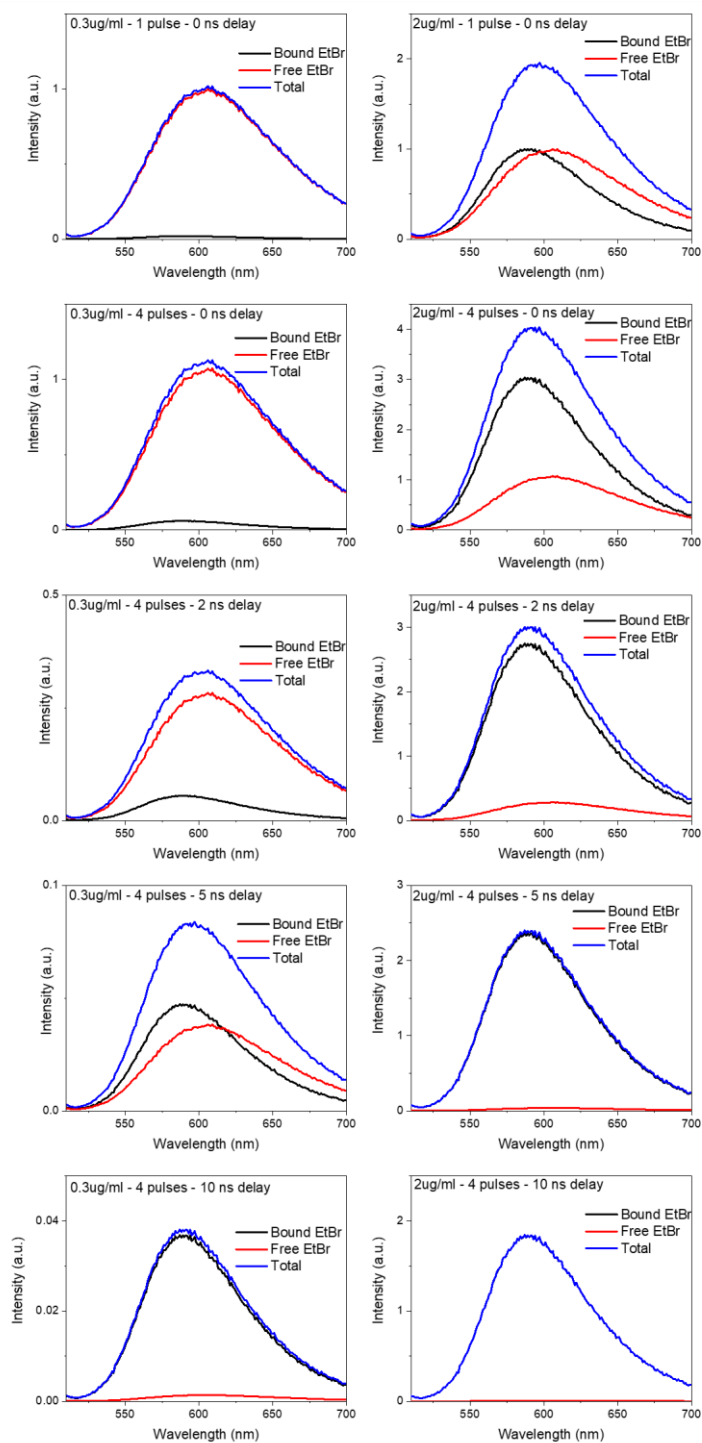There are two important conclusions to draw from these simulations. First, using a pulsed excitation mode, the signal from the target fraction (EtBr bound to DNA) is increased three-fold already for four pulses in the burst. Second, after more than a 5ns delay time in the gate opening, only the long-lived fraction (DNA bound EtBr) is detected. Consequently, since the intensity of the long-lived fraction (and total measured intensity) after more than 5ns is the only signal detected, collecting data under such conditions will exclusively reflect EtBr bound to DNA, which reveals the existence of DNA. At the same time, the intensity of the unwanted short-lived fraction is eliminated (the short-lived fraction was not enhanced by pulsing, and it has been heavily suppressed by time-gating).

2.5 Binding

Fluorescence is widely used in studying biological samples due to its generally non-destructive nature. The fluorescence measurement of some proteins can utilize the intrinsic structure of the protein, while other proteins can be "tagged" or "labeled" with an extrinsic fluorophore for the measurement. Biological samples can be measured, tracked, or analyzed using the steady state or time resolved (lifetime) fluorescence takes shift presented with emission and fluorescent lifetime.

Specifically, fluorescence detection of double-stranded DNA (dsDNA) takes advantage of the significant emission signal enhancement of dye-intercalators upon binding to DNA. Intercalation is the insertion of a molecule between DNA bases. The dye intercalates to DNA because of the limited access to water and stabilizes the dye's electronic states. This binding action typically shifts the extrinsic fluorophore's absorption spectrum and shifts its emission spectrum. The fluorescence signal enhancement resulted from the dye stabilization and manifests in an increased quantum yield and considerable fluorescence lifetime increase [30].

An excellent way to examine the binding of an intercalator to DNA is to consider a specific example. Using EtBr and DNA and exciting at 485 nm, we find that binding increases the fluorescence signal from EtBr about 5-fold. Furthermore, the emission of EtBr and EtBr bound to DNA has an emission shift of about 25nm, with the EtBr bound to DNA being blue-shifted, Figure 2.14.
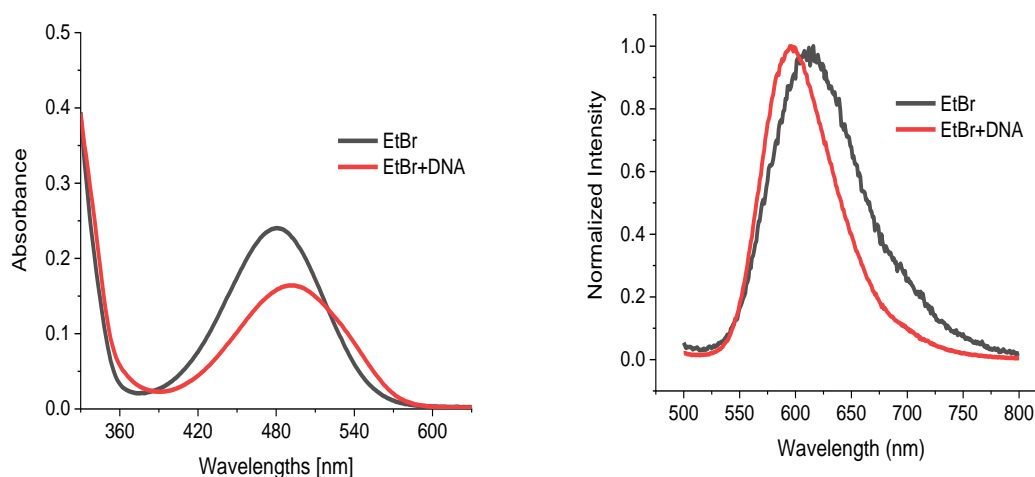
Figure 2.14. Absorption (left) and emission (right) spectra for free and DNA bound EtBr in PBS buffer.

The fluorescence intensity detected from the solution of EtBr containing DNA will be a simple composition of signal from free dye and signal from EtBr bound to DNA. The equilibrium between free and bound EtBr depends on the DNA and EtBr concentrations and the equilibrium dissociation constant, K_d . For simplicity, assume that the binding equilibrium can be found by assuming a single binding site. This assumption gives:

$$\theta = \frac{(K_d + C_1 + C_2) - [(K_d + C_1 + C_2)^2 - 4C_1C_2]^{1/2}}{2C_2} \quad (2.15)$$

Where θ represents a fraction of bound probe (EtBr) to a target (DNA), and C_1 and C_2 are concentrations of DNA and EtBr, respectively [12,15]. According to Equation 2.15, for a given concentration of EtBr, the fraction of EtBr bound to DNA initially increases linearly with increasing DNA concentration and then saturates (Figure 2.15). For the low initial EtBr concentration, the saturation increase is faster. So, typically to detect lower DNA concentrations, the use of very low EtBr concentrations is desirable. However, there is an essential factor to be considered. The initial signal of the probe (free EtBr) should be significantly higher than the background signal (electronic noise, dark counts, Raman signal, and background fluorescence of buffer or medium).
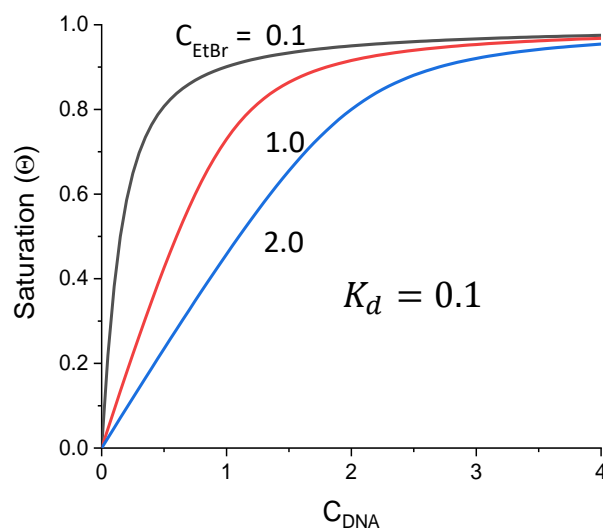
Figure 2.15. Example of theoretical binding curves. Saturation (θ) as function of DNA concentration for different concentrations of EtBr.

3. Methodology

3.1 DNA and EtBr Solutions

3.1.1 Materials
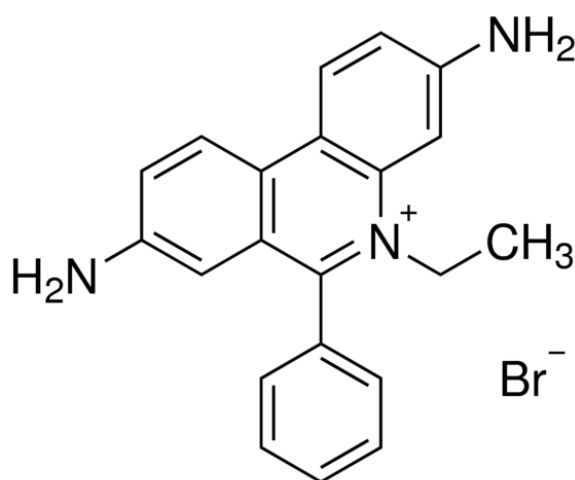
Figure 3.1. Structure of Ethidium Bromide from Sigma Aldrich [31].

The DNA and Ethidium Bromide (EtBr) were sourced from Sigma Aldrich (Inc). The CT DNA (Calf Thymus Deoxyribonucleic Acid) lyophilized powder was stored upon arrival at -18 °C. The EtBr was stored in powder form in dark storage at room temperature (~ 20 °C).

Stock solutions were made for DNA and EtBr. The DNA consisted of 1 bottle of the CT DNA to 20 ml of super deionized (DI) water. This 20 ml of super DI water was filtered with a 0.1 μm filter before use. The stock produced a concentration of ≈ 100 μg/ml that was then split into two vials, and one was stored in the freezer to be used later. The DNA vial that was left to be used was then wrapped in aluminum foil and kept in the dark storage at room temperature during the experiments. The EtBr was made into a stock solution using super DI water, again filtering it with a 0.1 μm filter before use. This stock was then diluted into a solution with an absorption < 0.2 A. U. .

3.1.2 Instrumentation

Absorption measurements were performed on the Cary 60 UV-Vis spectrometer using 0.2 cm quartz cuvettes. The absorption maximum for DNA was centered at 260 nm, and the absorption maximum was around 480 nm for Ethidium Bromide. All spectra were background corrected using super DI water filtered with the 0.1 μm filter as the solution.

3.2 Spectroscopic Measurements

3.2.1 Absorption, Emission, and Lifetime Measurements

UV-Vis absorption and steady state fluorescence spectra were obtained using a Cary 60 UV–visible Spectrophotometer (Varian Inc.) and Cary Eclipse Spectrofluorometer (Varian Inc.), respectively. Unless otherwise mentioned, all measurements were done in 2 mm x 1cm quartz cuvettes from Starna (Inc.).

Fluorescence emission spectra and lifetimes were measured on the FluoTime 300 fluorometer (PicoQuant, GmbH.) using a 485nm diode laser. The FT300 is equipped with an ultrafast microchannel PMT detector from Hamamatsu (Inc.). The Time Correlated Single Photon Counting (TCSPC) was done through a TimeHarp 260 (Picoquant, GmbH) module. The fluorescence lifetimes were measured. Lifetime data were analyzed using the FluoFit4 program from PicoQuant (GmbH.) using a multi-exponential fitting model for the intensity decay $I(t)$:

$$I(t) = \sum_i \alpha_i e^{-t/\tau_i} \quad (3.1)$$

where α_i is the fractional amplitude of the intensity decay of the ith component at time t and τ_i is the lifetime of the ith component. The intensity and amplitude weighted average lifetimes ($< \tau >_{int}$, and $< \tau >_{amp}$, respectively) were calculated using the following equations:

$$< \tau >_{int} = \sum_i f_i \tau_i \quad (3.2)$$

$$< \tau >_{amp} = \frac{\sum_i \alpha_i \tau_i}{\sum_i \alpha_i} \quad (3.3)$$

$$f_i = \frac{\alpha_i \tau_i}{\sum_i \alpha_i \tau_i} \quad (3.4)$$

Where f_i represents the fractional intensities for each fluorescence lifetime component.

The (normalized or reduced) χ^2 is the optimization parameter for the least-squares fitting analysis defined as:

$$\chi_R^2 = \frac{1}{n-p} \sum_{i=1}^{n} \left[\frac{I_i - I(t_i)}{\sigma_i} \right]^2 \quad (3.5)$$

Where n is the number of data points (number of total photons in the fluorescence decay), p is the number of freely varying parameters, σ_i is the standard deviation, I_i is the measured intensity at time t_i and $I(t_i)$ is the fitted theoretical value for the fitted intensity decay function at time t_i.

3.2.2 Multipulse

A multipulse system was designed using a 485 nm pulsed diode laser. A custom-made fiber optic was made for the multipulse system. The fiber splits into four branches, each equivalent in light output intensity, with the length of each branch increasing by about 75 cm. The excitation pulse is sent through the fiber, and the light splits into the four different branches that, in the end, come together to a single output. Each pulse travels a different optical path. At the output, four pulses are separated by about 4ns between each other, Figure 3.2.
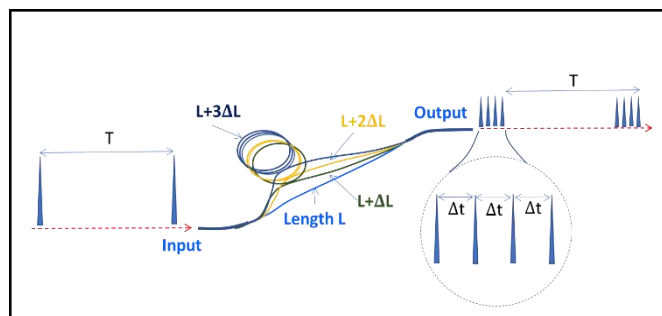
Figure 3.2. Schematic representation of the used fiber optics. The fiber splits into 4 equivalent branches, with the length of each branch increasing by about 75 cm.

The multipulse data was collected on Delta Flex (Horiba Inc.). The fluorometer is equipped with a Hybrid Picosecond Photon Detector (HPPD). The TCSPS was done using a FiPho (Horiba) module. Because we were calculating Time Resolved Emission Spectra (TRES), we wrote a code for the software instead of manually running the lifetimes. The creation of the code allowed us to run through a range of emission wavelengths while stopping to collect the lifetime at each selection.

This automation allows us to collect the lifetimes at the various emission wavelengths and automatically calculates the intensity counts under the intensity decay curve. The intensity counts under the decay curve are then used as points to recreate the emission spectra of the solution.

```
----------------------------------
--Set up dwell time and peak count
----------------------------------
ASSIGN DWELLTIME% = 0.2
ASSIGN PEAKIRF% = 0
----------------------------------
--Set up start/end and wavelength increment
----------------------------------
ASSIGN START% = 500
ASSIGN END% = 700
ASSIGN INC% = 10
CREATE MEASUREMENT [Sample Name Here]
----------------------------------
--IRF
----------------------------------
MESSAGE STOP Starting IRF measurement. Check scatter in sample holder.
MESSAGE IRF measurement.
MONOCHROMATOR EM1 WAVELENGTH 485 BANDPASS 2

MEASURE EM1 STOP 1 PEAK PEAKIRF% TIME 60 IRF NAME IRF
----------------------------------
--Set TRES sample
----------------------------------
MESSAGE STOP Starting TRES measurement. Put sample in holder and check
filters.
----------------------------------
--Loop over taking measurement changing wavelength
----------------------------------
LOOP WAVELENGTH% = START% TO END% BY INC%
      MONOCHROMATOR EM1 WAVELENGTH WAVELENGTH% BANDPASS 12
      MEASURE EM1 STOP 1 TIME 60 DWELLTIME% SECOND PEAK 0 DECAY NAME
WAVELENGTH%-DECAY
ENDLOOP
----------------------------------
--Calculate the TRES curves
----------------------------------
---CALCULATE TRES
----------------------------------
--declare end of script file
----------------------------------
END
```

Figure 3.3. Script written for Delta Flex (Horiba Inc.) to automate TRES experiments.

Figure 3.3 is the script created to automate the TRES experiments on the Delta Flex. The code starts by assigning general but necessary parameters for the experiment. The dwell time is the integration time for which the data is collected. It is recommended to make the dwell time at least ten times larger than the TCSPC window [32]. The peak IRF (instrument response function) is the max number of counts that the IRF peak can reach. For the code above, the dwell time is set to 0.2 ms, and the peak IRF is set to 0 as we will not be running the fluorescence decays a specific number of counts but rather a specific time. The next section of

the code above is the wavelength range the emission monochromator will scan over. The code starts at 500 nm and goes to 700 nm stopping every 10 nm for a fluorescence decay measurement. Ideally, the range is selected based on the peak and the width of the emission spectra of the sample. The measurement is then created where an appropriate name is given (ex. SampleName_2mmcuv_filters_λexc).

The next section of the code tells the Delta Flex information on the instrument response function (IRF) run. Here the code is written so that little pop-up boxes will show up to help direct the user through the process when it is run. The parameters for the IRF run in the code are then set; in this case, the emission monochromator is set to look at 485 nm with the bandpass slits set to 2 nm. The measurement is set to run for 60 seconds and will be labeled IRF when finished.

The fluorescent decay measurement is looped to run over the wavelengths assigned above. The measurement is set to run for 60 seconds for each decay, named "wavelength-decay" (ex. 500-decay). Again, the code is designed to have pop-up boxes to help instruct them through the setup. When the code finishes running the fluorescence decays, the TRES will be calculated using "CALCULATE TRES." The fluorescence decays and the TRES calculation are then shown on the screen.

3.2.3 Imaging

Laser excitation was provided by a pulsed diode laser, PDL-485 (Picoquant, GmbH), emitting a 485 nm light driven by a PDL 800 B (Picoquant, GmbH). This driver was operated at 1 MHz. Measurements were performed using a PI-Max (Princeton Instruments, Inc). The camera is synchronized with the pulsed diode laser. A 40 ns gate (time for which the detector remains open) was set to ensure that most photons emitted by EtBr with long (20 ns) lifetime were collected. The gate can be shifted as needed with 0.5 ns resolution. For observation, a 535 nm long-pass filter was used to eliminate the excitation light.

4. Results

4.1 Steady State Spectra

First, the absorption and emission spectra of free EtBr and EtBr bound to DNA in phosphate buffered saline (PBS) were measured in a 2 mm pathlength cuvette (Fig. 4.1 A and B).
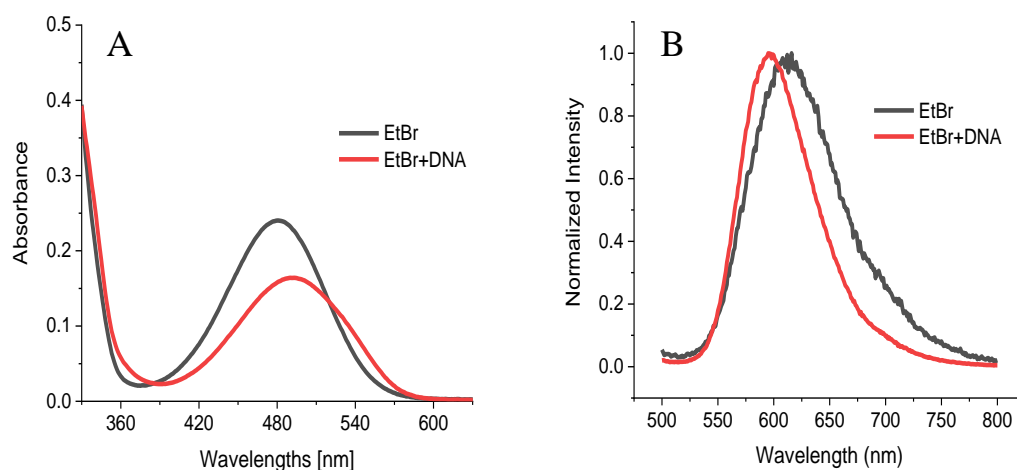

Figure 4.1. A. Absorption (left) and B. normalized emission (right) spectra for free and DNA bound EtBr in PBS buffer.

The emission spectra of free EtBr in PBS and EtBr saturated with DNA are shown in Figure 4.1 B. Raman scattering of the buffer using just PBS solution in identical instrumental settings was also measured. In Figure 4.2, the measured emission spectra for increasing concentrations of DNA are presented. The concentration of free EtBr in buffer was adjusted to result in an emission signal comparable to the Raman signal from water. In Figure 4.2, the solutions had increasing DNA concentrations (0, 40 ng/ml, 120 ng/ml, 240 ng/ml, 480 ng/ml, and 1440 ng/ml, respectively) [4].
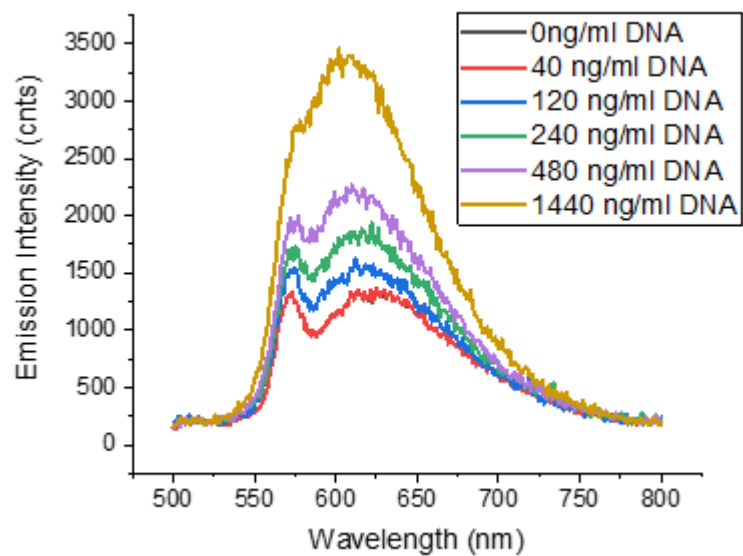
Figure 4.2. Emission spectra of solution of EtBr and various concentration of DNA. FT300 was used with 485 nm excitation.

4.2 Lifetimes

The FT-300 system allows for the measurement of fluorescence lifetimes and emission spectra (see above) in a cuvette in a single experiment without a change in setup. The intensity decay curves were already discussed in section 2.4 and have been reported in [1,12]. The intensity decay of free EtBr is fast, with a fluorescence lifetime of about 1.5 ns, and the fluorescence lifetime of EtBr, when bound to DNA, is much longer, about 20 ns, see Figure 4.3.
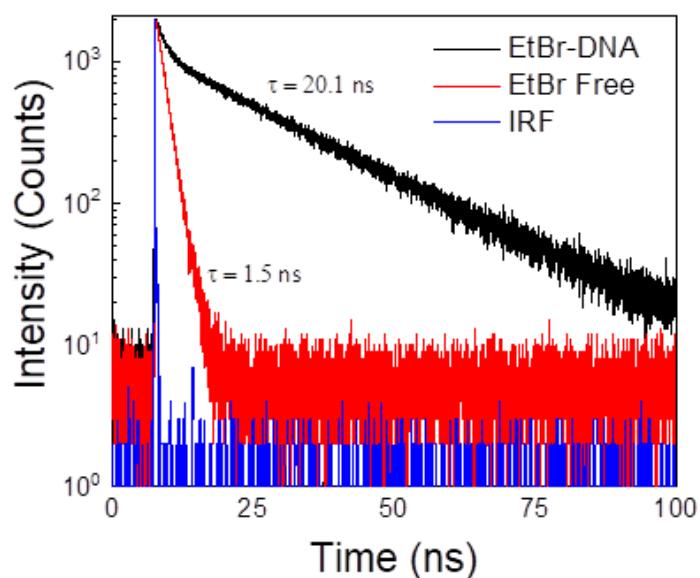
Figure 4.3. Fluorescence intensity decays for EtBr (red) and EtBr bound to DNA (blue).

Next, the EtBr bound with DNA was mixed with the free EtBr at an arbitrary amount to demonstrate the lifetime solution with free EtBr and bound EtBr would look like (Figure 4.4).
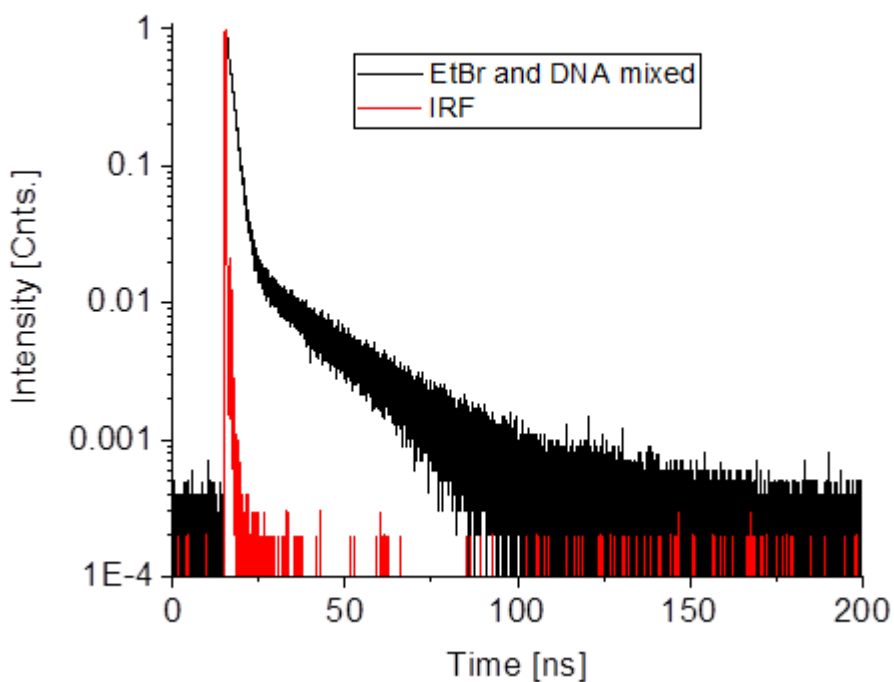

Figure 4.4. Fluorescence intensity decay of EtBr free and EtBr bound to DNA mixed. The EtBr free is the short component in the beginning of the decay and the EtBr bound to DNA is the long component that starts to dominate around ≈ 10ns.

4.3 Multipulse

Figure 4.5A presents a burst of four pulses as measured from ludox scattering Figure 4.5B presents a burst as measured with free EtBr solution, and Figure 4.5C a burst as measured from an EtBr solution saturated with DNA (~95 ng/ul). It is difficult to couple the light to the fiber so that the intensity of each pulse in the burst will be identical. In practice, the intensity between pulses in the burst varies slightly. The first pulse is about 30% stronger (see Figure 4.5A), but it does not change during the experiment, and the bursts are identical over time. The fluorescence intensity between pulses as measured from free EtBr solution (1.5 ns fluorescence lifetime) does not change from pulse-to-pulse, and fluorescence intensity decays almost to zero after each pulse (Figure 4.5B). However, for DNA-bound EtBr (20 ns fluorescence lifetime), the intensity increases from pulse-to-pulse.

Figure 4.5. Burst of 4 pulses as measured in time correlated single photon counting (TCSPC) system (Delta Flex from Horiba Inc.): A. Ludox scattering (0 fluorescence lifetime), B. Emission of free EtBr solution (1.5 ns fluorescence lifetime), and C. Emission from a solution of EtBr that is saturated with DNA (~95 ng/ul).

After four pulses, it is three times higher than the initial intensity after one pulse. Starting photon collection after the fourth pulse (triggering a detector with a delay) will enhance the

signal of the long component (DNA bound EtBr) in relation to the signal from free EtBr, which will significantly increase the sensitivity for detecting the long-lived fraction.

Time-Resolved Emission Spectra (TRES) (Figure 2.2) were measured for both single pulse excitation and four pulse excitation for a free EtBr solution Figure 4.6. The various lifetimes collected with one pulse will be used in the background for the four pulses and will be subtracted to leave only the long-lived component. TRES with concentrations of 95 µg/ml, 2 µg/ml, 0.6 µg/ml, 0.3 µg/ml and 0 µg/ml of DNA were measured.
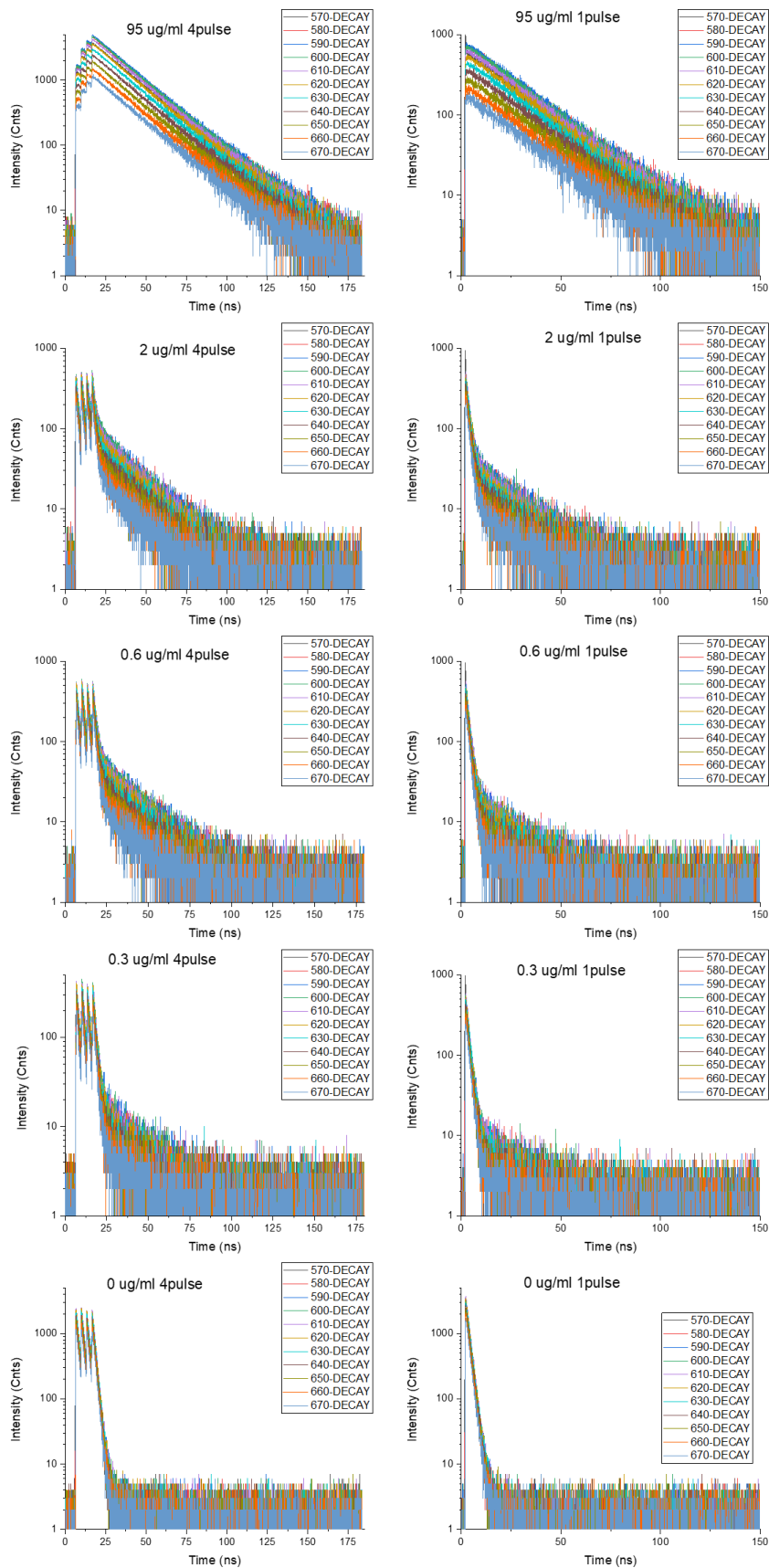
Figure 4.6. Fluorescence Decays of various DNA amounts (95 μg/ml, 2 μg/ml, 0.6 μg/ml, 0.3 μg/ml and 0 μg/ml) over ten different emission wavelengths from 570 nm-670 nm. Left column is four pulse excitation lifetimes, and the right column is 1 pulse excitation lifetimes.

4.4 Imaging

Two solutions of low DNA concentration (0.3 ng/μl and 0.15 ng/μl) were tested to assess the possibility of applying pulsed excitation and time-gated detection to expose small amounts of DNA present in a sample. Three small dents were drilled on a teflon cuvette cap to produce three wells, as seen in Figure 4.7. Each well can be filled with about 2- 3 μl of solution.

The wells were filled with ~2.5 μl of buffer (as a reference), free EtBr solution, and
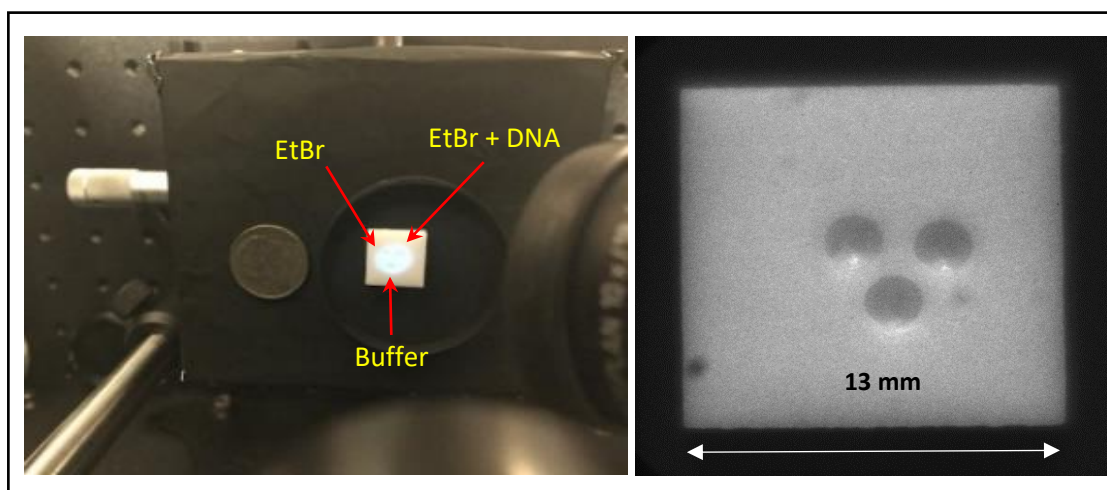
Figure 4.7. Time-delayed images of three wells filed with buffer, EtBr solution, and EtBr solutions with different amounts of DNA. Left – photography of imaging stage with teflon cuvette cap with three drilled small dents in the center. Right - camera image of the cap acquired with the 5X objective utilized for the experiment.

DNA/EtBr solution as marked in Figure 4.7, respectively. An amount of ~ 2.5 ul of the DNA/EtBr solution of 0.3 ng/μl contains about 750 pg of DNA (higher concentration), and when filled with the lower concentration solution (0.15 ng/μl), about 375 pg of DNA. Excitation from a 485 nm laser through a fiber that produces a 4-pulse burst was used, as presented in Figure 3.1. The excitation laser repetition rate was one MHz (corresponding to the highest repetition rate accepted by the camera), leading to 4-pulse bursts separated by one microsecond.

The photograph in Figure 4.7 shows the experimental setup with three wells illuminated with the excitation beam. On the left side of the photograph, a dime is positioned for size reference. A 5x objective was used to image the wells. On the right side, the image field is shown as seen by the camera (an ambient light photograph taken by the imaging camera) where

the wells are visible. The camera is synchronized with the pulsed laser. A 40 ns gate (time for which the detector remains open) was set to ensure that most photons emitted by EtBr with long (20 ns) lifetime will be collected. The gate can be shifted as needed with 0.5 ns resolution. For observation, a 535 nm long-pass filter was used to eliminate the excitation light.

5. Analysis

5.1 Absorption Analysis

Different concentrations of EtBr in deionized (DI) water were used to estimate the detection limits for our spectrometer. Ideally, when selecting the proper wavelength excitation for the emission spectra, the goal is to select the wavelength where the absorption is at least 50% or greater than the peak absorption (the peak wavelength for EtBr in water is around 480 nm, as shown in Figure 5.1A). In an ideal case, the excitation wavelength selected should have a larger absorbance for EtBr bound to DNA than for free EtBr. Figure 5.1B is the ratio of bound EtBr vs. free EtBr. The shaded regions show where the absorbance of bound EtBr is at least 50% of the max absorbance at 480 nm.
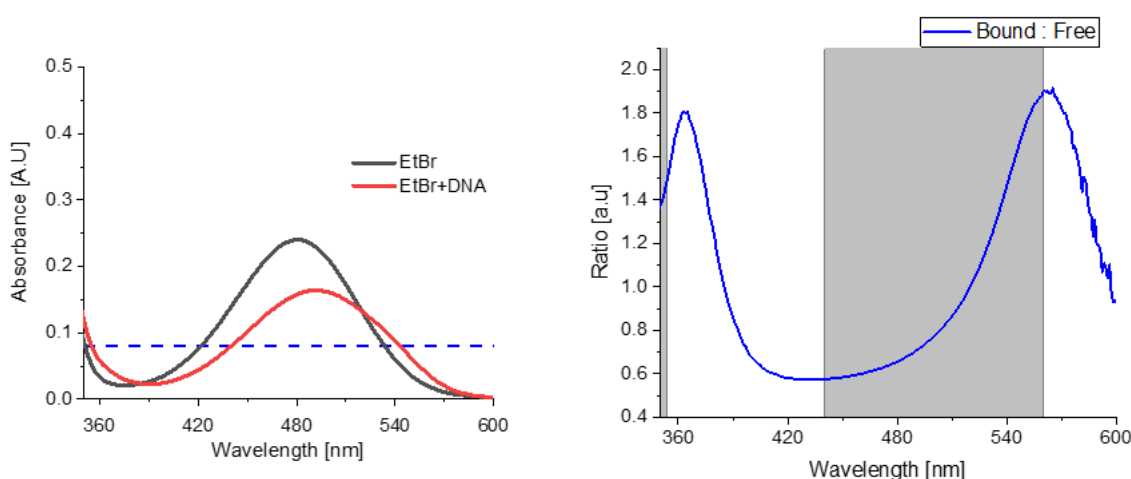

Figure 5.1. A. (left) is absorption of EtBr free (black line) and EtBr with DNA (red line). The blue dashed line marks where absorbance is 50% or great than the peak absorbance of EtBr with DNA at 485nm. B. (right) is the ratio of EtBr with DNA to EtBr free. The grey shaded region represents where the absorbance is above the blue dashed line on 5.1.A.

Figure 5.1B shows the excitation range that should be used is between 520-540 nm, as it is in the shaded region and is a local maximum for the selection. The Raman signal from water is typically used as a standard for comparing a detector's sensitivity [33]. The low concentration of DNA and dye used in these experiments make it vital to know the water Raman signal. Although selecting an excitation in the range of 520-540nm would make the signal from bound EtBr much more prominent (Figure 5.1A), the water Raman line overlaps with the dye's emission spectrum. The selected 485 nm excitation wavelength, chosen due to its proximity to the max absorption of bound EtBr, presents water Raman scattering at about 555 nm, just before the EtBr emission spectrum. When using 485 nm excitation, the EtBr concentration can be minimized/adjusted so the observed Raman peak will be visible in front of the emission spectrum. The minimum concentration of EtBr (no DNA) is selected to give a comparable signal at maximum emission to the water Raman peak maximum (see Figure 5.4A). This will allow for the easy reproduction of the experiment in any independent instrumentation since the Raman signal of water is constant.

5.2 Emission Analysis

Raman scattering of water using just PBS solution in identical instrumental settings was also measured. In Figure 5.2A-F, the measured emission spectra for increasing concentrations of DNA (points) are presented. Spectral decomposition was used to estimate the sensitivity limit for detecting DNA. In Figure 5.2, the measured spectra (points) and results for the spectral decomposition using three components were included; the baseline (Raman), free EtBr, and EtBr saturated with DNA. All measured emission spectra for EtBr solution with different DNA concentrations are simple compositions of the emission spectrum of free EtBr, the emission spectrum of EtBr bound to DNA, Raman water signal, and instrumental baseline. In Figure 5.2, the recovered EtBr fractions (free and bound) for increasing DNA concentrations (0, 40 ng/ml, 120 ng/ml, 240 ng/ml, 480 ng/ml, and 1440 ng/ml, respectively) are presented.

Figure 5.2B shows the lowest concentration of DNA (40 ng/ml) that can be distinguished from the experimental baseline. We found that the DNA concentrations 20 ng/ml and below are not distinguishable by analysis, in which an example is shown in Figure 5.2A. In the case of 20 ng/ml of DNA or lower, the spectral decomposition typically reflects a small trace of EtBr bound to DNA within experimental error. The dilution of DNA below 40 ng/ml does not show any change in the emission spectra or the fitted components. Concentrations of less than 40 ng/ml of DNA are below the detection threshold for the FT-300, and the analysis cannot distinguish EtBr bound to DNA from a baseline and free EtBr in the solution. Therefore, the concentration range 40 - 80 ng/ml is considered the detection limit (Figure 5.2B & 5.2C). Further increases in concentration produce substantial changes in emission and spectral deconvolution that reflects DNA bound EtBr.
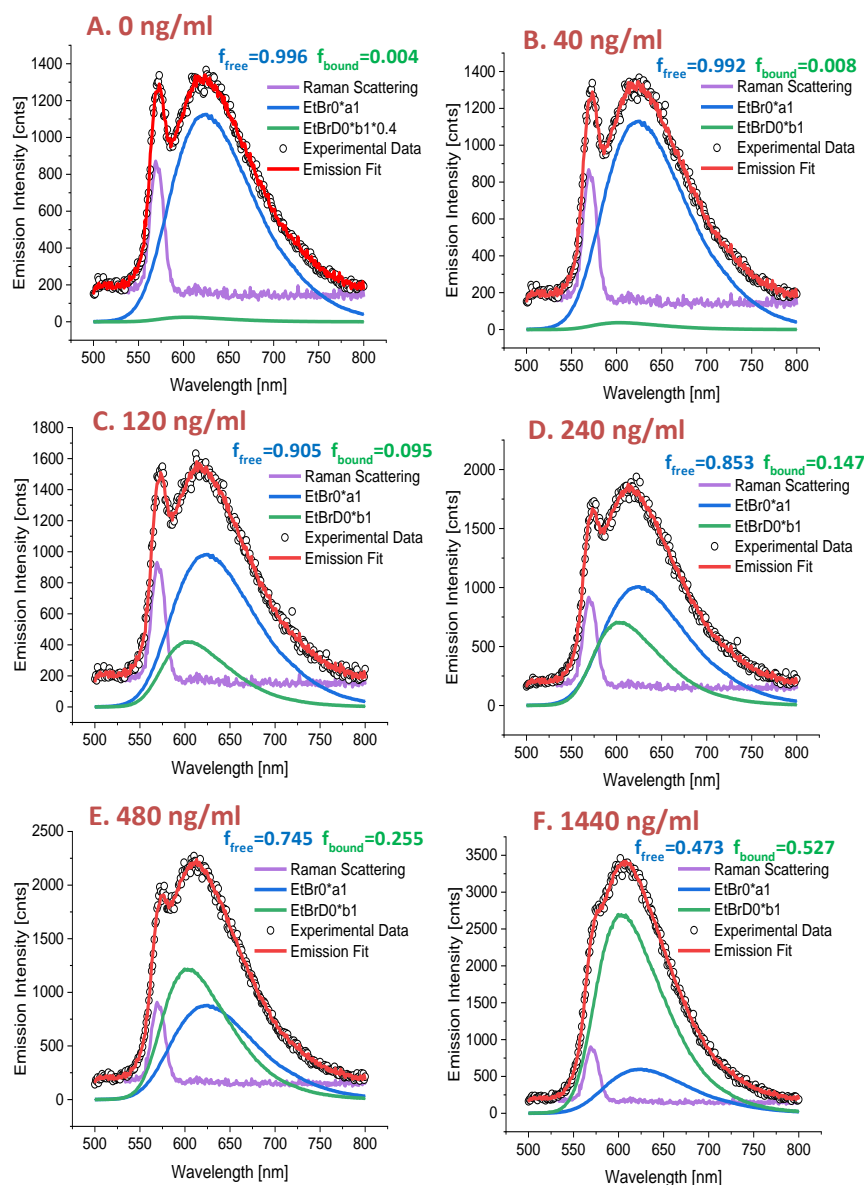
Figure 5.2. The absorption and emission spectra of free EtBr and EtBr bound to DNA measured in 2mm path cuvette.

Furthermore, our excitation beam focuses on the spot size below 0.5 mm² giving a detection volume of about or below 1 µl. This corresponds to the amount of detectable DNA, which is approximately about or below 80 pg. Therefore, by crude estimation, it appears that less than 100 pg of DNA can be detected if positioned in the center of detection.

5.3 Multipulse Analysis

The TRES script (Figure 3.2) collects the lifetimes (Figure 4.7). Then the script takes integrals of the decays summing up the number of photons counted for each emission wavelength, thus allowing them to become points used to recreate a "time-resolved" emission spectrum (TRES). We can use this code to select the time delay over which the lifetime is being integrated, representing a change in the information of the long-lived component.

The first column of Figure 5.3 shows that the highest concentration of DNA is 2ng/μl, corresponding to about 3% of EtBr bound to DNA (97% of free EtBr in solution). When applying four pulse burst excitation (see Figure 5.3 first column), the intensity fraction increases after each pulse. After the fourth pulse, the long-lived fraction constitutes about 75% of the total signal at the initial time. As the time delay increases, the short-lived fraction quickly decays. After a 10ns delay, the signal of the long component completely dominates (only the signal from the long component is detected).
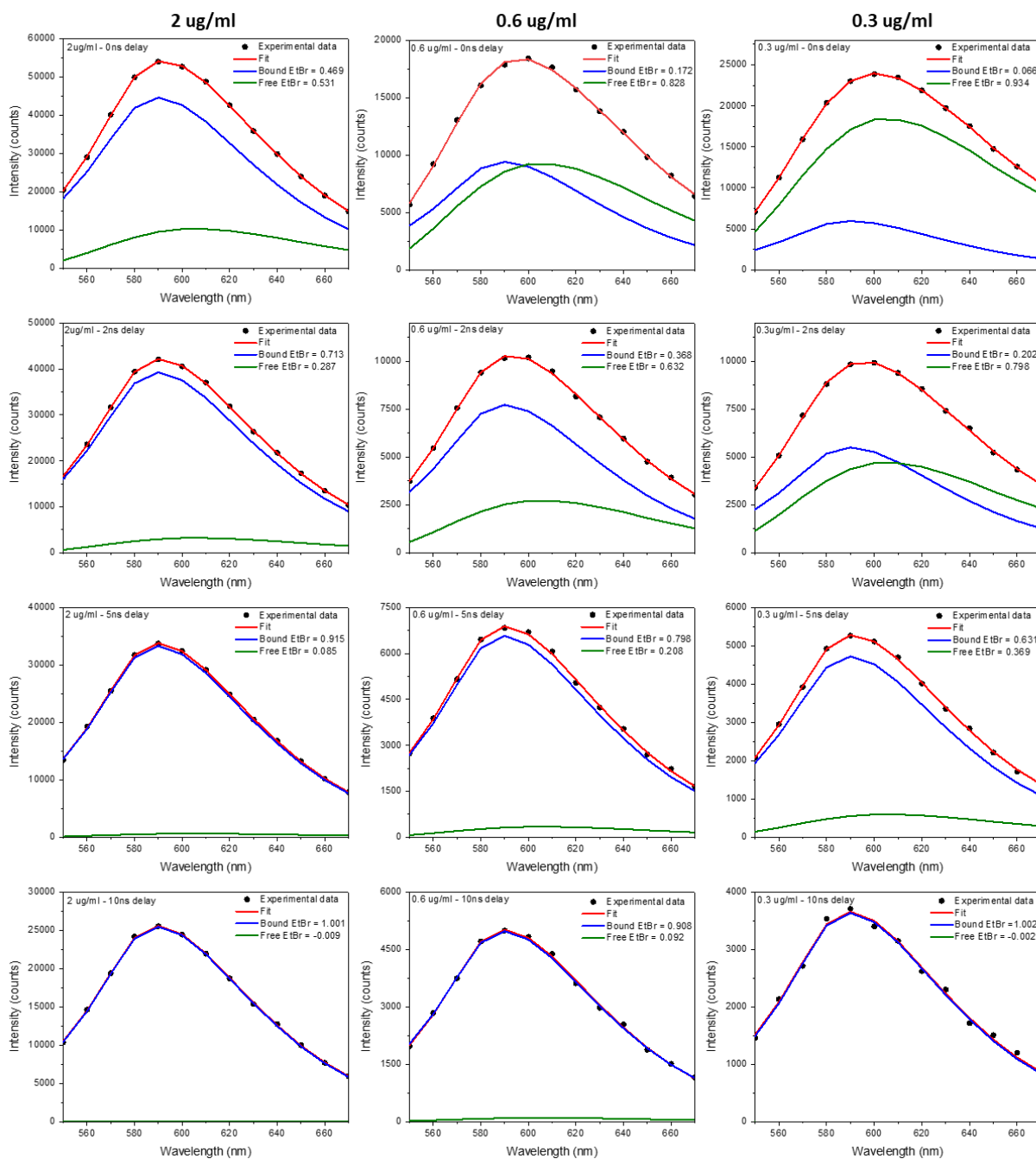
Figure 5.3. Time Resolved Emission Spectra (TRES) as measured with four pulse excitations burst after a time delay of 0 ns, 2 ns, 5 ns, and 10 ns after the last pulse in the burst, respectively for three DNA concentrations 2, 0.6 and 0.3 ug/ml (the concentration of EtBr is kept constant for each DNA concentration).

For a lower concentration of 0.6 ng/μl (Figure 5.3 middle column), the bound fraction is less than 1%, and the apparent initial fraction of the long-lived component after the fourth pulse in the burst is slightly more than 17%. The relative fraction of the long component (EtBr bound to DNA) increases quickly for an increasing delay for the gate opening. After 10 ns, the

intensity fraction of the bound component is over 95%. Again, the same is demonstrated for an even lower concentration of 0.3 ng/µl (Figure 5.3 right column). The overall signal is lower for lower DNA concentration, but after 10ns, only the long-lived fraction (EtBr bound to DNA) is visible.

In all cases, the intensity fraction of the long-lived component between zero ns time delay and 10ns time delay drops less than 50%, while for short-lived component falls almost to zero (over 99.5%). So, even starting with a dominant fraction of short-lived component (over 99%), the detected signal after four pulse excitation and delay of 10ns or longer would only be due to the bound fraction.

5.4 Imaging

With the camera, we collected images for different delays of the gate opening, as shown in Figure 5.4. The initial time assignment (0 ns) corresponds to a time shift, after which the image intensity starts dropping down. One must remember that the actual delay depends on the time delay between the pulse reaching the sample and the synchronization (camera triggering signal) activating the camera. Since the physical gate cannot be instantaneously opened and the rise time is in the order of nanoseconds, even a short-lived 1.5 ns decay will be spread over time. The top row of images shows EtBr only (in the left well) and EtBr with ~750 pg of DNA (in the right well). The lower well filled with buffer is invisible, showing that background is eliminated (suppressed by taking a background image and subtracting it). At time zero ns, the image of the well containing DNA is slightly brighter due to the small amount of DNA-bound fraction. As the gate opening time is delayed (keeping the gate width of 40 ns constant), the

brightness of the left well quickly disappears, and for delays longer than 15 ns, the left well is entirely invisible.
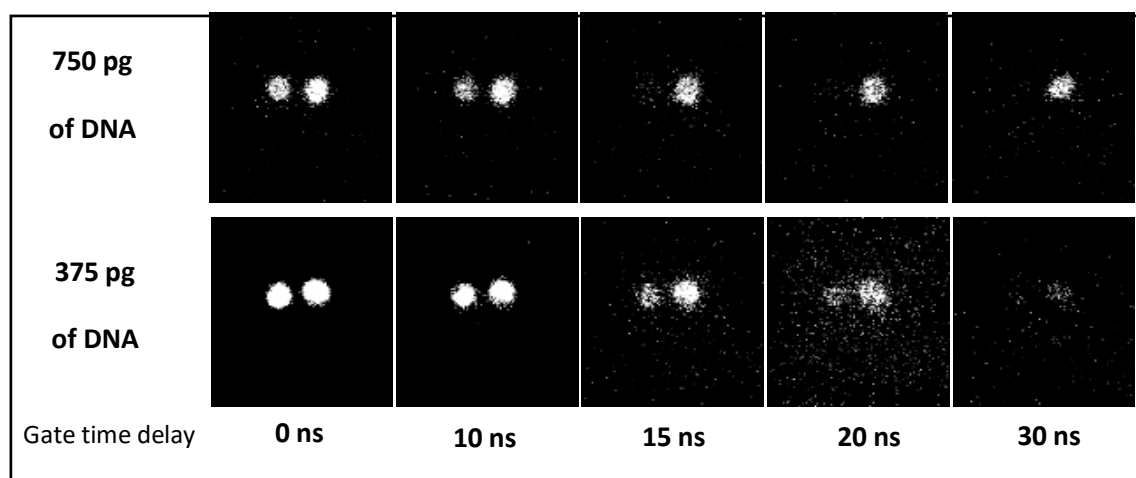
Figure 5.4. Time-delayed images of three wells filed with buffer, EtBr solution, and EtBr solutions with different amounts of DNA. The images collected are for different delays of gate opening time for two different amounts of DNA in the right well.

In contrast, the brightness of the right well-containing DNA drops only 50%. The lower row of images shows the same time lapses but for only 375 pg of DNA. The initial brightness (zero ns time) for EtBr only and EtBr with DNA are practically equal. However, by increasing the time delay, the left well disappears much faster. Since the image intensifier gain and the number of collected frames to detect images need to be increased, the free EtBr is visible longer. However, collecting each image still takes less than 5 seconds. Notably, the well with the buffer (background) is not visible even with the increased sensitivity.

6. Conclusion

Currently, the optimum input for sample enrichment (i.e., Polymerase Chain Reaction) before allele detection is 500 to 1,000 pg of DNA, which is equivalent to $80 - 160$ diploid cells (approximately 6 pg/cell [34]). However, due to advances and increased sensitivity of DNA typing methods, DNA profiles can be analyzed from low template DNA samples [35,36]. With trace DNA concentrations, partial DNA profiles can be obtained, which still can provide significant evidence in criminal and missing person cases.

In this paper, we presented approaches that demonstrate the potential of significant sensitivity enhancement for detecting small amounts of DNA. The first method used steady state emission spectra based on the spectral change induced by an intercalator binding to DNA [4]. Spectral decomposition was applied to the overall emission signals to extract the fraction of EtBr bound to DNA. We were able to detect down to 120 ng/ml of DNA in the cuvette using EtBr.

We then utilized the change in fluorescence lifetime of an intercalator upon binding to DNA [12] and a change in the emission spectrum through advanced multipulse technology. We used two approaches to isolate and enhance this change in fluorescence lifetime, time gating and advanced multipulse technology. This approach is more technologically advanced but is easily achievable in a typical laboratory setup. With cuvette solutions, we were able to detect down to 0.3 µg/ml of DNA. And when imaging is applied in tandem with this approach, we can detect 375 pg of DNA in a 3 µl well.

These strategies open a new direction for quick visualization of minute amounts of DNA in a sample. The capability to visualize sub-nanograms amounts of DNA in microliters of the solution is demonstrated.

The detection sensitivity that we found could be significantly increased in the future by using a higher power excitation laser diode and/or by utilizing a laser diode with an excitation wavelength of 540 nm or even 560 nm preferentially excites EtBr bound to DNA. In addition, EtBr is a well-characterized model system for these experiments and by applying these new technologies to dyes that may exhibit much higher sensitivity of DNA staining (e.g., Ethidium homodimer, YOYO, or Diamond^{TM}), the sensitivity of detection can be efficiently increased by an order of magnitude, and thus single picograms of DNA could be easily visualized.

The ability to detect picograms of DNA can make the analysis DNA much more efficient. Additionally, such an easy and capable approach can be immediately utilized as a sensitive and versatile method for DNA localization that does not destroy the structure of DNA during detection. But furthermore, using improved quick visualization can be especially valuable for DNA extraction and DNA recovery from complex surfaces as bones [37] and other challenging samples as hair [38].

The presented results open the doorway to a novel approach to localize DNA on a swab or any touched object or surface. This is a proof-of-concept approach testing the assumption that by using simple spectral analysis and a convenient DNA intercalator, it could be possible to detect/localize DNA on a solid/complex surface. To demonstrate this potential, three swabs, as shown in Figure 6.1 a green laser pointer (535 nm), and a regular smartphone to take pictures were assessed. The detection was performed at a low level of room light, and swabs are visible in orange color. On the center swab, DNA was applied to two spots and EtBr was applied to the center and right swab. Through the 575 nm long-pass filter swabs in orange color and no green excitation (it is eliminated by the filter) can be seen.

This demonstrates a clear and simple approach that can push the current limits of DNA detection and make important contributions to the forensic and biotechnology field.

Figure 6.1. *Photography of three collecting swabs. The swabs were illuminated by a 535 nm laser as seen by the 575 nm long pass filter. DNA was put in two spots on the middle swab. EtBr was then applied to the center and right swab.*

Bibliography

1. Z. Gryczynski, and I. Gryczynski, *Practical Fluorescence* (CRC Press- Taylor & Francis Group, Boca Raton, Fl. 2020).
2. J.R. Lakowicz, *Principles of Fluorescence Spectroscopy*, (Springer Science, New York, NY, 2006).
3. B. Valeur and M.N. Barberan-Santos, *Molecular Fluorescence: Principles and Applications* (Hoboken, New Jersey, United States of America: Wiley-VCH, 2012).
4. E. Kitchner et al. Analyst, **146**, 1198 (2021)
5. F. M. Pohl, et al. Proc. Natl. Acad. Sci., **69**, 3805 (1972)
6. J. Markovits, B.P. Roques, and J-L. Le Pecq. Anal. Biochem., **94**, 259 (1979)
7. J. M. Kelly, et al. Nucleic Acids Res., **13**, 6017 (1985)
8. A. Glazer, N. K. Peck, and R.A Mathies., Proc. Natl. Acad. Sci., **8**, 3851 (1990)
9. S. Gurrieri, et al. Ann. Biochem. **249**, 44 (1997)
10. S. Nafisi, et al. **35**, 827 (2007)
11. R. Chib et al., Methods Appl. Fluorescence, **2**, 1(2014)
12. J.D. Kimball et al. Analyst, **143**, 2819 (2018).
13. L. Ceresa et al. Analyst (2021)
14. F. Ma, Y. Li, B. Tang, C.Y. Zhang, Acc Chem Res, **49**(9), 1722 (2016)
15. P. Kanokwongnuwut, P. Kirkbride, and A. Linacre, Forensic Science International, **291**, 115 (2018).
16. P. Kanokwongnuwut, K.P. Kirkbride, and A. Linacre, Forensic Science International Genetics, **37**, 95 (2018)
17. B. Budowle, D. L. Hobson, J. B. Smerick, and J. A. L. Smith, Twelfth International Symposium on Human Identification,
18. P. Gill, Croat. Med. J., **42**, 229 (2001).
19. P. Gill et al., Forensic Science International, **112**, 17 (2000).
20. Z. Gryczynski, I. Gryczynski, and J.R. Lakowicz, Meth. of Enzymology, **360**, 41 (2003)
21. V. Sharma, et al., Biomedical Optics Express, **3** (8), 1825 (2012)
22. A. Ziegler, et al., Hum Genet, **131**(10), 1627, (2012).
23. J. Kimball, Ph.D. Thesis, Texas Christian University, 2015, (online TCU Library)
24. L. Ceresa, M.S. Thesis, Texas Christian University, 2020, (online TCU Library)
25. D. Jameson, *Introduction to Fluorescence* (CRC Press, Taylor & Francis Group, Boca Raton, Florida, 2014)
26. D. Shumilov et al., Methods Appl. Fluoresc. **2** (024009), 9pp (2014)
27. R.M. Rich, et al., Methods Appl. Fluoresc., **66**, 292 (2014).
28. R. Fudala, et al., SS FLUOR, **15**, 1 (2014).
29. Kimball et al., *Multipulse Excitation for Enhanced Fluorescence Detection,* SRS Poster, (2014).
30. H. Sahoo, RSC Adv., **2**, 7017 (2012)
31. Sigma Aldrich, *Ethidium Bromide*, (https://www.sigmaaldrich.com/US/en/product/sial/e8751?context=product)
32. V. Buschmann, et al., PicoQuant Technical Note, *PLIM Practical Ascpects* (2016)
33. Horiba, *How to Calculate Signal to Noise Ratio*, (https://www.horiba.com/en_en /technology/spectroscopy/fluorescence-spectroscopy/how-to-calculate-signal-to-noise-ratio/)
34. C. Baumer et al, Sci Rep, 8(1), 7476 (2018).
35. C. Borsting, H.S. Mogensen, N. Morling. Forensic Sci Int Genet, 7(3), 345 (2013).

36. M. M. Buś, et al., BioTechniques, Accepted, June 2021.
37. A. Margaryan, et al., Nature, 585, 390 (2020).
38. M. Almeida, et al., Forensic Sci Int Genet, 3, e319 (2011)

Note: Passages in this thesis have been quoted verbatim from the following sources:
E. Kitchner et al. *A novel approach for visualization and localization of small amounts of DNA on swabs to improve DNA collection and recovery process.* Analyst (2021)

L. Ceresa et al. *A Novel Approach to Imaging and Visualization of Minute Amounts of DNA in Small Volume Samples.* Analyst (2021)

All figures were reprinted with permission from the Royal Society of Chemistry.

VITA

Personal background	Emma Lynne Kitchner
	Hudson Fall, NY
	Daughter of Peter and Kimberly Kitchner
Education	Advanced Regents Diploma, Hudson Falls High School, NY, 2015
	Bachelor of Science, Physics and Mathematics, St. Lawrence University, NY, USA, 2019
	Master of Science, Physics, Texas Christian University, Fort Worth, TX, USA, 2021
Experience	Teaching Assistant, Texas Christian University, Fort Worth, TX, USA, 2019-2021
	Teaching Assistant, St. Lawrence University, Canton, NY, USA, 2017-2019
Awards	Green Fellowship, 2019

ABSTRACT

DNA Detection: Finding the Limits

Emma Kitchner M.S. 2021

Department of Physics and Astronomy

Texas Christian University

Research Advisor: Dr. Karol Gryczynski, W.A. "Tex" Moncrief, Jr. Chair of Physics

Detecting and monitoring of low amounts of DNA is crucial for many biomedical and forensic applications. Improving detection sensitivity becomes then a central goal of DNA-based testing and diagnostics. In this thesis, we look at three approaches (steady state emission, fluorescence lifetime, and advanced multipulse detection) that demonstrates the potential for significant sensitivity enhancement for detecting small amounts of DNA. These methods are straightforward and are used in accompaniment with spectral decomposition using a standard DNA intercalator: Ethidium Bromide (EtBr). The developed techniques can be applied to various other intercalators and ultimately in practical applications. This will allow for better decision-making in clinical medicine, biological and environmental research, and human identification in forensic investigations.